Time-course of sodium transport along the nephron in nephrotic syndrome: the role of potassium

Dizin, Eva ; Olivier, Valérie ; Maire, Charline ; Komarynets, Olga ; Sassi, Ali ; Roth, Isabelle ; Loffing, Johannes ; de Seigneux, Sophie ; Maillard, Marc ; Rutkowski, Joseph M ; Edwards, Aurélie ; Feraille, Eric

Abstract: The mechanism of sodium retention and its location in kidney tubules may vary with time in nephrotic syndrome (NS). We studied the mechanisms of sodium retention in transgenic POD-ATTAC mice, which display an inducible podocyte-specific apoptosis. At day 2 after the induction of NS, the increased abundance of NHE3 and phosphorylated NCC in nephrotic mice compared with controls suggest that early sodium retention occurs mainly in the proximal and distal tubules. At day 3, the abundance of NHE3 normalized, phosphorylated NCC levels decreased, and cleavage and apical localization of -ENaC increased in nephrotic mice. These findings indicate that sodium retention shifted from the proximal and distal tubules to the collecting system. Increased cleavage and apical localization of -ENaC persisted at day 5 in nephrotic mice when hypovolemia resolved and steady-state was reached. Sodium retention and -ENaC cleavage were independent of the increased plasma levels of aldosterone. Nephrotic mice displayed decreased glomerular filtration rate and urinary potassium excretion associated with hyperkaliemia at day 3. Feeding nephrotic mice with a low potassium diet prevented hyperkaliemia, -ENaC cleavage, and led to persistent increased phosphorylation of NCC. These results suggest that potassium homeostasis is a major determinant of the tubular site of sodium retention in nephrotic mice.

DOI: https://doi.org/10.1096/fj.201901345r

Received: 4 June 2019 | Revised: 21 November 2019 | Accepted: 30 November 2019

DOI: 10.1096/fj.201901345R

RESEARCH ARTICLE

THE FASEB JOURNAL

Time-course of sodium transport along the nephron in nephrotic syndrome: The role of potassium

Eva Dizin[1,2] | Valérie Olivier[1,2] | Charline Maire[1,2] | Olga Komarynets[1] | Ali Sassi[1] | Isabelle Roth[1,2] | Johannes Loffing[2,3] | Sophie de Seigneux[1,2] | Marc Maillard[4] | Joseph M. Rutkowski[5] | Aurélie Edwards[6] | Eric Feraille[1,2]

[1]Department of Cellular Physiology and Metabolism, University of Geneva, CMU, Geneva, Switzerland

[2]National Centre of Competence in Research "Kidney.ch", Zürich, Switzerland

[3]Institute of Anatomy, University of Zürich, Zürich, Switzerland

[4]Service of Nephrology, Centre Hospitalier Universitaire Vaudois, Lausanne, Switzerland

[5]Department of Medical Physiology, Texas A&M University Health Science Center, Bryan, TX, USA

[6]Department of Biomedical Engineering, Boston University, Boston, MA, USA

Correspondence
Eric Feraille, Department of Cellular Physiology and Metabolism, Faculty of Medicine, University of Geneva, CMU, 1 Rue Michel Servet, Geneva 4 1211, Switzerland.
Email: Eric.Feraille@unige.ch

Funding information
Swiss National Science Foundation, Grant/Award Number: 31003A_156736/1; Swiss National Science Foundation, Grant/Award Number: 310030_143929/1

Abstract

The mechanism of sodium retention and its location in kidney tubules may vary with time in nephrotic syndrome (NS). We studied the mechanisms of sodium retention in transgenic POD-ATTAC mice, which display an inducible podocyte-specific apoptosis. At day 2 after the induction of NS, the increased abundance of NHE3 and phosphorylated NCC in nephrotic mice compared with controls suggest that early sodium retention occurs mainly in the proximal and distal tubules. At day 3, the abundance of NHE3 normalized, phosphorylated NCC levels decreased, and cleavage and apical localization of γ-ENaC increased in nephrotic mice. These findings indicate that sodium retention shifted from the proximal and distal tubules to the collecting system. Increased cleavage and apical localization of γ-ENaC persisted at day 5 in nephrotic mice when hypovolemia resolved and steady-state was reached. Sodium retention and γ-ENaC cleavage were independent of the increased plasma levels of aldosterone. Nephrotic mice displayed decreased glomerular filtration rate and urinary potassium excretion associated with hyperkaliemia at day 3. Feeding nephrotic mice with a low potassium diet prevented hyperkaliemia, γ-ENaC cleavage, and led to persistent increased phosphorylation of NCC. These results suggest that potassium homeostasis is a major determinant of the tubular site of sodium retention in nephrotic mice.

KEYWORDS

aldosterone paradox, edema, ENaC, hyperkalemia, proteinuria, SRAA

Abbreviations: ASDN, aldoterone-sensitive distal nephron; AQP-2, aquaporin-2; CCD, cortical collecting duct; CD, collecting duct; DCT, distal collecting duct, ENaC, epithelial sodium channel; MR, mineralocorticoid receptor; NCC, sodium-chloride cotransporter; NKCC, sodium-potassium-chloride cotransporter; NS, nephrotic syndrome; PAN, puromycin aminonucleoside; PCT, proximal convoluted tubule; RAAS, renin-angiotensin-aldosterone system; TAL, thick ascending limb of Henle.

Eva Dizin and Valérie Olivier these authors contributed equally to this work.

1 | INTRODUCTION

The mechanisms of edema formation in nephrotic syndrome (NS) have long been a subject of investigation.[1] The "underfilling" hypothesis postulates that proteinuria and subsequent hypoalbuminemia lead to decreased intravascular oncotic pressure, altering Starling forces and inducing a transfer of water and solutes from plasma into the interstitial space, leading to hypovolemia. The ensuing activation of the Renin-Angiotensin-Aldosterone System (RAAS) results in secondary renal retention of sodium (and therefore water) by activation of ENaC in the connecting tubules and collecting ducts.[2] The "overfilling" hypothesis states that proteinuria itself can cause primary sodium retention via the direct processing and activation of γ-ENaC by urinary serine proteases.[3] Thus, the aldosterone-sensitive distal nephron (ASDN) is thought to be the principal site of sodium retention. Indeed, increased Na,K-ATPase expression and activity have been consistently reported in the cortical collecting duct (CCD) of proteinuric rats.[4] ENaC seems to be a key player in sodium retention in NS, and aldosterone seems to play a permissive role in ENaC activation. The expression and apical targeting of ENaC have been observed to increase in an aldosterone-dependent manner in the CCD of proteinuric rats.[5,6] Moreover, increased apical ENaC targeting has not been observed in adrenalectomized puromycin aminonucleoside (PAN) nephrotic rats with clamped plasma aldosterone, even when they still displayed amiloride-sensitive sodium retention.[6,7]

The underfilling and overfilling hypotheses are not mutually exclusive since the one or the other mechanism may dominate depending on the development stage of NS, the rate of hypoproteinemia and the absolute plasma oncotic pressure. Current experimental models of NS have severe limitations. Most studies have been conducted in rats injected with toxic substances such as PAN, which induces massive proteinuria and sodium retention but also damages kidney tubules.[6] In addition, knock-out mouse models for podocyte-specific proteins such as nephrin[8] or podocin,[9] which are required for the integrity of the glomerular filtration barrier, display massive perinatal lethality and/or severe renal failure that precludes their utilization as models of idiopathic NS.

In order to circumvent these problems, we used the POD-ATTAC transgenic mouse model, in which NS stems from an inducible podocyte-specific apoptosis,[10] to test our hypothesis that different mechanisms drive sodium retention depending on hemodynamics and the development phase of NS.

2 | METHODS

2.1 | Animal experiments

All animal experiments were approved by the Institutional Ethical Committee of Animal Care of the University of Geneva and Cantonal authorities.

POD-ATTAC transgenic mice kindly provided by Dr. Scherer (Southwestern Texas University, Dallas, TX) were bred and housed in the animal facility of the Faculty of Medicine of Geneva. Genotyping of transgenic mice was performed by PCR analysis of ear biopsies using the following primers: forward, 5′- GAA AGT GCC CAA ACT TCA GAG CAT TAG G - 3′ and reverse, 5′ - AAC TGA GAT GTC AGC TCA TAG ATG GGG G - 3′. NS was induced by intraperitoneal injection of 0.5 μg/g body weight of the chemical dimerizer, AP20187 (Takara Bio Inc. Kusatsu, Japan), in 8-10 weeks old male transgenic mice. Male wild-type littermates were used as controls and were injected with the same dose of chemical dimerizer.

Mice were individually housed in metabolic cages (Tecniplast, Buguggiate, Italy). Water and food (Provimi-Kliba, Kaiseraugst, Switzerland) containing normal (1.55% wt/wt) or low (0.01% wt/wt) potassium were provided *ad libitum*. After 1 d of adaptation, food and water intake, body weight, and 24 hours urine volume were recorded daily. Urine was collected each day till day 5 after dimerizer injection for chemical analysis. On the 2nd, 3rd, or 5th day after dimerizer injection, mice were anesthetized by 100 mg/kg ketamine and 5 mg/kg xylazine (Bayer Healthcare, Berlin, Germany). Blood was collected via the submandibular vein for chemical analysis, ascites was weighed on an absorptive tissue after the opening of the peritoneal cavity, and kidneys were removed before sacrifice by lethal bleeding. Kidneys were either fixed by immersion in 4% paraformaldehyde for histological analysis or frozen in liquid nitrogen and stored at -80% for subsequent RNA and protein extraction.

2.2 | Biological parameters

Blood parameters (sodium, potassium, chloride, bicarbonate, creatinine, hematocrit) were measured on day 2, 3, or 5 using the Epoc technology (Siemens Healthcare, Erlangen, Germany). Urinary sodium, potassium, chloride, and creatinine concentrations were measured using a UniCel DxC800 Synchron Clinical System automated analyzer (Beckman Coulter, Brea, CA). Plasma and urinary proteins were measured with a Konelab automated analyzer (Thermo-Fisher, Waltham, MA). Results are expressed in mmol/l except protein concentrations, which are expressed in g/L. The urinary protein/creatinine ratio was

calculated for normalized with respect to the volume of urine excretion. Plasma aldosterone levels were measured according to standard procedures using a radioimmunoassay (Coat-A-Count RIA kit; Siemens Medical Solutions Diagnostics, Ballerup, Denmark). Results are means ± SEM.

2.3 | Glomerular filtration rate

Mice were anesthetized with isoflurane and a miniaturized imager device (Mannheim Pharma and Diagnostics, Mannheim, Germany) was mounted onto the animal's back. The skin background signal was recorded for 5 minutes before intravenous injection of 150 mg/kg FITC-sinistrin (Mannheim Pharma and Diagnostics, Germany). Then, transcutaneous fluorescence was recorded for 1h in conscious animals. mGFR (μL/min) was calculated from the decrease in fluorescence intensity over time (ie, plasma half-life of FITC-sinistrin) using a two-compartment model, the mouse body weight and an empirical conversion factor using the MPD Lab software (Mannheim Pharma and Diagnostics, Germany), as previously described.[11] Results are means ± SEM.

2.4 | Functional diuretic tests

For diuretic response studies, we performed an intraperitoneal injection of hydrochlorothiazide (50 mg/kg) to inhibit NCC or benzamil (5 mg/kg) to inhibit ENaC, as previously described.[12] Urinary Na^+ excretion was measured 24 hours before and 24 hours after diuretic administration. Results are expressed as a ratio of urinary sodium/urinary creatinine concentrations after or before diuretic administration and as means ± SEM.

2.5 | MR antagonist

Potassium canrenoate (Sigma-Aldrich, Saint Louis, MI, USA) was used as a mineralocorticoid receptor (MR) antagonist. POD ATTAC and FVB (Friend leukemia virus B) mice were treated with daily subcutaneous injection of canrenoate (50 mg/kg) starting the day before the injection of the dimerizer, until sacrifice on the 3rd day after dimerizer injection.

2.6 | RNA extraction and real-time qPCR

Total RNA was extracted from kidney and hypothalamus tissues using the NucleoSpin RNA II kit (Macherey-Nagel, Düren, Germany) according to the manufacturer instructions. Five hundred nanograms of RNA were used to synthesize cDNA using the qScript cDNA Supermix (Quantabio, Gaithersburg, MD). Real-time PCR was performed on 10 ng of cDNA using 0.5 mM of each primer, 6 μL of SYBR Green Master Mix (Applied Biosystems) and 2 μL of water to obtain a final reaction volume of 12 μL. The primers used are described in Table 1. Mouse acidic ribosomal phosphoprotein, P0, was used as the internal standard except where otherwise noted. Duplicate amplification reactions were performed with an ABI prism 7000 Sequence Detection System (Applied Biosystems). Fold difference in cDNA abundance (F) was calculated using the formula $F = 2^{(Ct1-Ct2)}$, where Ct1 and Ct2 are the number of cycles required to reach the threshold of amplicon abundance for experimental and control conditions, respectively. Normalization to one control animal was performed to assess biological variability in both controls and nephrotic groups. Results were expressed as fold of control ± SEM.

2.7 | Western blotting

Kidney tissues were lysed as previously described.[13] Proteins were quantified using a BCA protein assay kit (Pierce, Rockford, Il), and subjected to SDS-PAGE and blotted onto polyvinylidene difluoride membranes (Immobilon-P; Millipore, Bedford, MA) using standard methods. The antibodies used are indicated in Table 2. Protein signals were quantified with image J software. Results are expressed as the ratio of the densitometry of the band of interest to the loading control or to the Coomassie blue staining. Then

TABLE 1 Primers for qRT-PCR

Name	Forward	Reverse
NHE3	CAG GTG GTC ACC TTC AAA TG	GGG ACA GGT GAA AGA CGA TT
NKCC2	TGG GTT GTC AAC TTC TGC AA	GCT CCG GGA AAT CAG GTA GT
NCC	ACC ACC ATC TCC TAC CTT GC	GGA GTC ATG GTG TCG TTC AC
α-ENaC	CAG ACT TGG AGC TTT GAC AAG GA	ACT TCT CTG TGC CTT GTT TAT ATG TGT T
β-ENaC	CAG ACT GGG CCT ATT GCT ATC TAA A	ACA TGC TGA GGC AGG TCT CTC T
γ-ENaC	CCG AGA TCG AGA CAG CAA TGT	CGC TCA GCT TGA AGG ATT CTG
AQP2	CAT GAG ATT ACC CCT GTA GAA ATC C	CGG CTG TTG CAT TGT TGT G
Vasopressin	TCG CCA GGA TGC TCA ACA CT	GGA AGT AGC AGG CGG AGG AG
SGK1	CCA AAC CCT CCG ACT TTC AC	CCT TGT GCC TAG CCA GAA GAA

TABLE 2 Antibodies used for Western blots

Name	Specie	Dilution	Supplier	Reference
NHE3	Rabbit	1/1000	StressMarq	41
NKCC2	Rabbit	1/1000	J Loffing	42
NCC	Rabbit	1/1000	J Loffing	43
NCC-pT53	Rabbit	1/1000	J Loffing	43
NCC-pT58	Rabbit	1/1000	J Loffing	43
α-ENaC	Rabbit	1/1000	J Loffing	42
β-ENaC	Rabbit	1/1000	StressMarq Biosciences	Ref SPC-404
γ-ENaC	Rabbit	1/1000	StressMarq Biosciences	Ref SPC405
AQP2	Rabbit	1/1000	RW Schrier	37
E-Cadherin	Mouse	1/2000	BD Biosciences	Ref 610404
β-actin	Mouse	1/10000	Sigma	A5441
SPAK	Rabbit	1/100	Millipore	07-2271
SPAK-pSer373	Rabbit	1/500	Millipore	07-2273

normalization to one control animal was also performed to assess biological variability in both controls and nephrotic groups. Results were expressed as fold of control ± SEM.

Coomassie blue staining was performed on urine samples in order to detect the proteinuria of POD-ATTAC mice. Each day following dimerizer injection, urine samples from FVB and POD-ATTAC mice were taken, pooled, and diluted (1:20) for comparison to a standard consisting of serial dilutions of bovine serum albumin (BSA). Urine pools and BSA solutions were then denatured by heating for 5 minutes at 95°C and loaded into polyacrylamide gel for SDS-PAGE.

2.8 | Immunofluorescence

Paraformaldehyde-fixed kidneys were dehydrated and paraffin-embedded. Kidney sections of 5 μm thickness were used for analysis. Non-specific binding was blocked with normal goat serum 2% for 20 minutes. The sections were incubated with primary antibody (Table 2) (diluted in PBS with 2% BSA) overnight at 4°C and then incubated 1 h with a secondary fluorescent antibody (goat anti-rabbit IgG AlexaFluor 488) at room temperature. Samples were mounted on microscope slides using Vectashield mounting medium (Maravai Life Science, San Diego, CA, USA) with DAPI for nuclear counterstaining. Fluorescence images were acquired using a LSM 710 confocal laser-scanning microscope (Carl Zeiss, Oberkochen, Germany). Z-stack images were summarized using ImageJ software (National institute of Health, US).

2.9 | Mathematical modeling of Na^+ transport along the nephron

Model predictions of transepithelial sodium fluxes and oxygen consumption rates were obtained using a published model of transport along the superficial nephron of a rat.[12,14] Tubular sodium transport and oxygen consumption rates are expressed in mmol/h/100 *g* body weight to allow for a direct comparison between rat and mouse data.

2.10 | Statistics

Results are given as the mean ± SEM from *n* independent experiments. Prism version 7.02 (GraphPad Software, San Diego,California,USA) was used for statistical analysis. The normal distribution of the population from which sample data was extracted was determined by a Shapiro-Wilk test. For parametric data, statistical differences were assessed using a two-tailed unpaired *t* test for comparison between two groups or one-way ANOVA with multipair wise comparison from Tukey for comparisons between more than two groups. For non-parametric data, statistical differences were assessed using the Mann-Whitney test for comparison between two groups or by the Kruskal-Wallis test with a multipair wise comparison from Dunn for comparisons between more than two groups. A *P*- value <.05 was considered significant.

3 | RESULTS

3.1 | POD-ATTAC mice rapidly developed nephrotic syndrome

After dimerizer injection, POD-ATTAC mice rapidly developed nephrotic proteinuria mainly composed of albumin as detected by Coomassie blue staining (Figure 1A). Proteinuria started at day 2 after dimerizer injection, became massive at day 3 and remained stable until at least the 5th day (Figure 1B). In parallel, plasma protein concentration

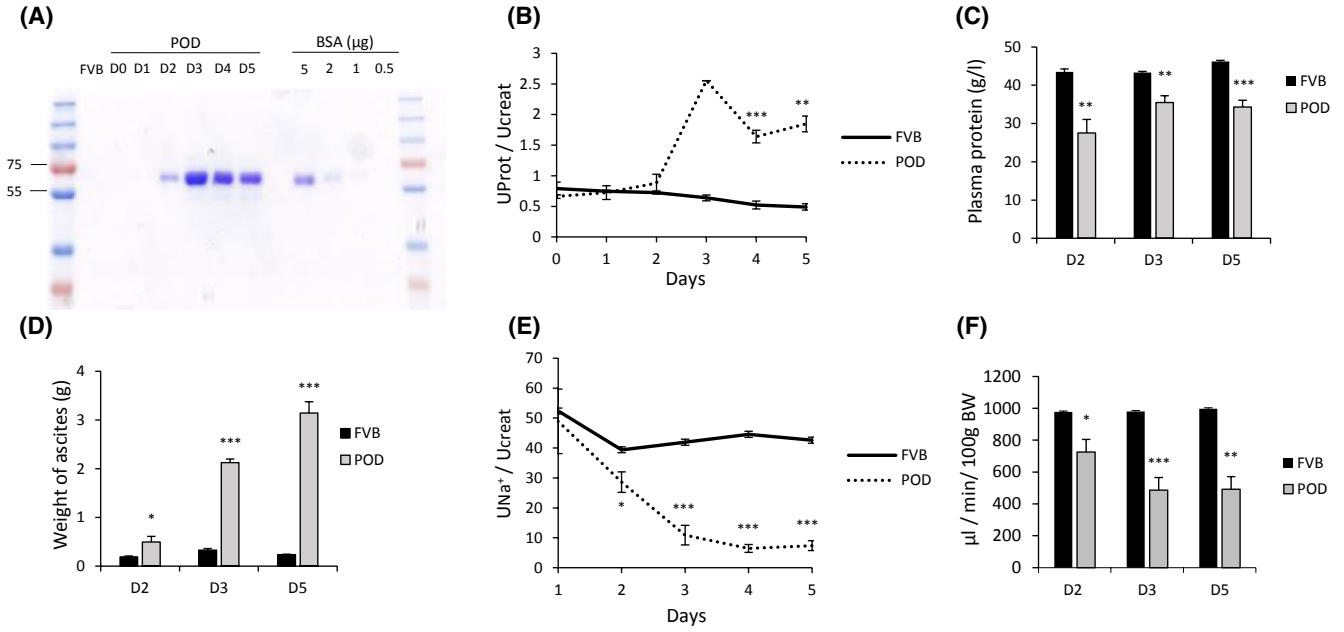

FIGURE 1 Nephrotic syndrome in POD-ATTAC mice. A, Proteinuria mainly composed of albumin was detected by Coomassie blue staining after SDS-PAGE in urine from POD-ATTAC (POD) mice, which was absent in control (FVB) mice. Increasing concentrations of BSA were loaded as a control of protein size. B, Time-course of proteinuria, expressed as the ratio proteinuria (in g/L) over creatininuria (in g/L), C, plasma protein concentration (g/L), D, weight of ascites (g), E, urinary sodium excretion expressed as the ratio of urinary sodium (in mmol/L) over creatininuria (in mmol/lL), and F, glomerular filtration rate in POD and FVB mice after intraperitoneal administration of dimerizer. Values are means ± SEM from 1 to 14 mice in each group. Statistical differences between control mice and POD-ATTAC mice were assessed using an unpaired Student *t* test; $*P < .05$, $**P < .01$, $***P < .001$

was decreased from days 2 to day 5 (Figure 1C). Proteinuria was associated with the development of ascites, decreased natriuresis and weight gain (Figure 1D,E, Supplementary Figure 1C) starting at day 2 and indicated large sodium and fluid retention.

Both hematocrit and blood hemoglobin concentration were increased at day 2 and 3 in proteinuric mice as compared to control mice (Table 3), indicating the contraction of circulating volume at the onset of NS. Ascites was associated with decreased natremia starting at day 2 and becoming significant at day 3. This finding suggests that expansion of extracellular volume was due to both primary sodium and water retention during this early phase (Figure 1 and Table 3). On the 5th day after dimerizer injection, proteinuria, and hypoproteinemia persisted but hematocrit, hemoglobin, and natremia were normalized when compared to control mice after massive sodium retention and ascites (Figure 1 and Table 3). Finally, POD-ATTAC mice displayed an early and progressive decrease in GFR after the induction of proteinuria, becoming apparent at day 2, maximal at day 3 and remaining stable until day 5 (Figure 1F). This decreased GFR was associated with decreased urinary potassium excretion (Figure 9A) and hyperkalemia (Table 3) starting at day 3 and sustained until day 5.

3.2 | Increased expression levels of NHE3 and phosphorylation of NCC are present at the onset of NS

Experiments performed at day 2 after the injection of dimerizer in POD-ATTAC mice revealed an altered expression pattern of nephron segment-specific sodium transporters. The protein abundance of NHE3, a sodium transporter that is mostly expressed along the proximal tubule, was strongly increased in POD-ATTAC mice (percentage of controls ± SEM: 335 ± 65.6) (Figure 2A,B). In the distal convoluted tubule (DCT), the total NCC protein abundance remained unchanged while phosphorylated NCC levels increased by in nephrotic mice as compared to control mice (percentage of controls ± SEM: 431.2 ± 73.5) (Figure 2A,B). Immunofluorescence staining showed the apical localization of phosphorylated NCC in both control FVB and POD-ATTAC nephrotic mice (Figure 2D). The abundance of NKCC2 protein expressed along the thick ascending limb of Henle (TAL) was not significantly increased and that of β-ENaC and full-length γ-ENaC proteins expressed along the connecting tubule (CNT) and collecting duct (CD) was unchanged. However, α-ENaC protein abundance was significantly decreased and the abundance of the cleaved form of γ-ENaC protein started to rise in POD-ATTAC mice. Figure

TABLE 3 Plasma parameters in FVB and POD-ATTAC mice 2, 3, and 5 days after NS induction

	FVB			POD		
	D2	D3	D5	D2	D3	D5
Na^+ (mM)	154.5 ± 1.32 (4)	156.75 ± 1.13 (6)	156.33 ± 2.09 (6)	148.25 ± 2.87 (4)	149.75 ± 2.17 (4)*	156 ± 0.93 (6)
K^+ (mM)	4.3 ± 0.25 (4)	3.9 ± 0.10 (6)	3.9 ± 0.25 (6)	4.95 ± 0.3 (4)	6.05 ± 0.78 (4)**	5.45 ± 0.31 (6)**
pH	7.09 ± 0.04 (4)	7.15 ± 0.02 (6)	7.13 ± 0.01 (6)	7.15 ± 0.01 (4)	7.16 ± 0.01(4)	7.15 ± 0.02 (6)
HCO_3^- (mM)	26.53 ± 1.46 (4)	27.97 ± 0.31 (6)	29.13 ± 0.53 (6)	27.28 ± 0.34 (4)	25.52 ± 1.12(4)*	27.58 ± 0.77 (6)
Hct (%)	35.5 ± 0.87 (4)	34.5 ± 0.54 (6)	38.5 ± 0.67 (6)	39.75 ± 1.38* (4)	37.5 ± 0.5 (4)*	36.66 ± 1.38 (6)
Hgb (g/dL)	12.03 ± 0.28 (4)	11.72 ± 0.19 (6)	13.08 ± 0.25 (6)	13.58 ± 0.5* (4)	12.82 ± 0.14 (4)*	12.46 ± 0.49 (6)

Note: Results are means ± SEM from 4-6 animals. Statistical differences between FVB and POD-ATTAC mice at each day and for each biological parameter were assessed using an unpaired Student *t* test.

*$P < .05$; **$P < .01$.

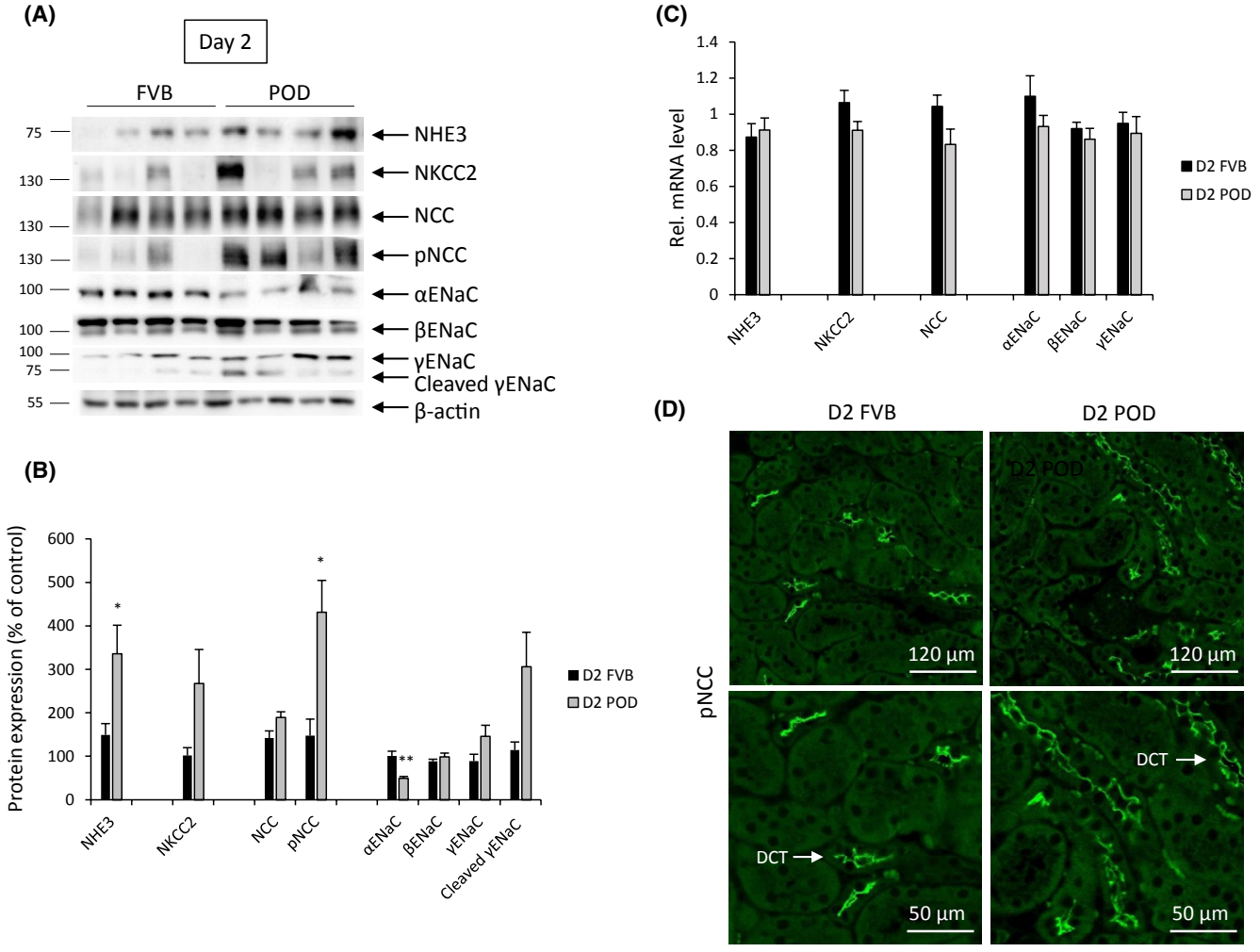

FIGURE 2 Early activation of NCC in nephrotic syndrome. Two days after intraperitoneal injection of dimerizer, kidneys from nephrotic POD-ATTAC (POD), and control (FVB) mice were harvested. Total proteins and RNA were extracted from kidney cortices and proteins were separated by SDS-PAGE. Kidney slices were fixed by immersion and processed for immunohistochemistry. A, Representative Western blot experiment showing the abundance of total and post-translationally modified kidney tubule sodium transporters, namely: NHE3, NKCC2, total and phosphorylated (TP53) NCC, α and β-ENaC, and full-length and cleaved γ-ENaC. β-actin was used as a loading control. B, Bar graph shows the densitometric quantification of Western blots. C, qRT-PCR analysis of variations in the mRNA levels of the main tubular sodium transporters. D, Immunofluorescence imaging of phosphorylated (TP58) NCC shows increased staining in the distal convoluted tubules (DCT) of nephrotic POD mice. Values are means ± SEM from 4 mice in each group. POD-ATTAC were compared to control mice using an unpaired Student *t* test; *$P < .05$, **$P < .01$, ***$P < .001$

2C shows that in contrast to protein levels, the mRNA levels of all the sodium transporters studied remained unchanged in nephrotic mice as compared with control mice indicating that increased NHE3 protein levels are most likely due to decreased protein degradation.

3.3 | Decreased NCC phosphorylation and increased γ-ENaC cleavage correlates with massive sodium retention

At day 3 after the injection of dimerizer in POD-ATTAC mice, a different expression pattern of nephron segment-specific sodium transporters was observed. Experiments revealed a massive increase in the cleaved form of γ-ENaC (percentage of controls ± SEM: 403 ± 101.1) associated with a decrease in full-length γ-ENaC abundance (percentage of controls ± SEM: 34 ± 7.7) (Figure 3A,B) and increased apical staining of γ-ENaC in the CNT and CD (Figure 3D) in POD-ATTAC mice. In contrast, the abundance of NCC protein and its phosphorylated form was dramatically decreased during this phase (percentage of controls ± SEM: 52.4 ± 8.1 and 36.6 ± 3 .9 for NCC and phosphorylated NCC respectively) while NHE3 protein abundance returned to baseline levels in nephrotic mice (Figure 3A,B). The mRNA levels of NKCC2, NCC, β-, and γ-ENaC were significantly decreased (Figure 3C) suggesting a negative feedback on sodium transporters and channels gene transcription or mRNA degradation.

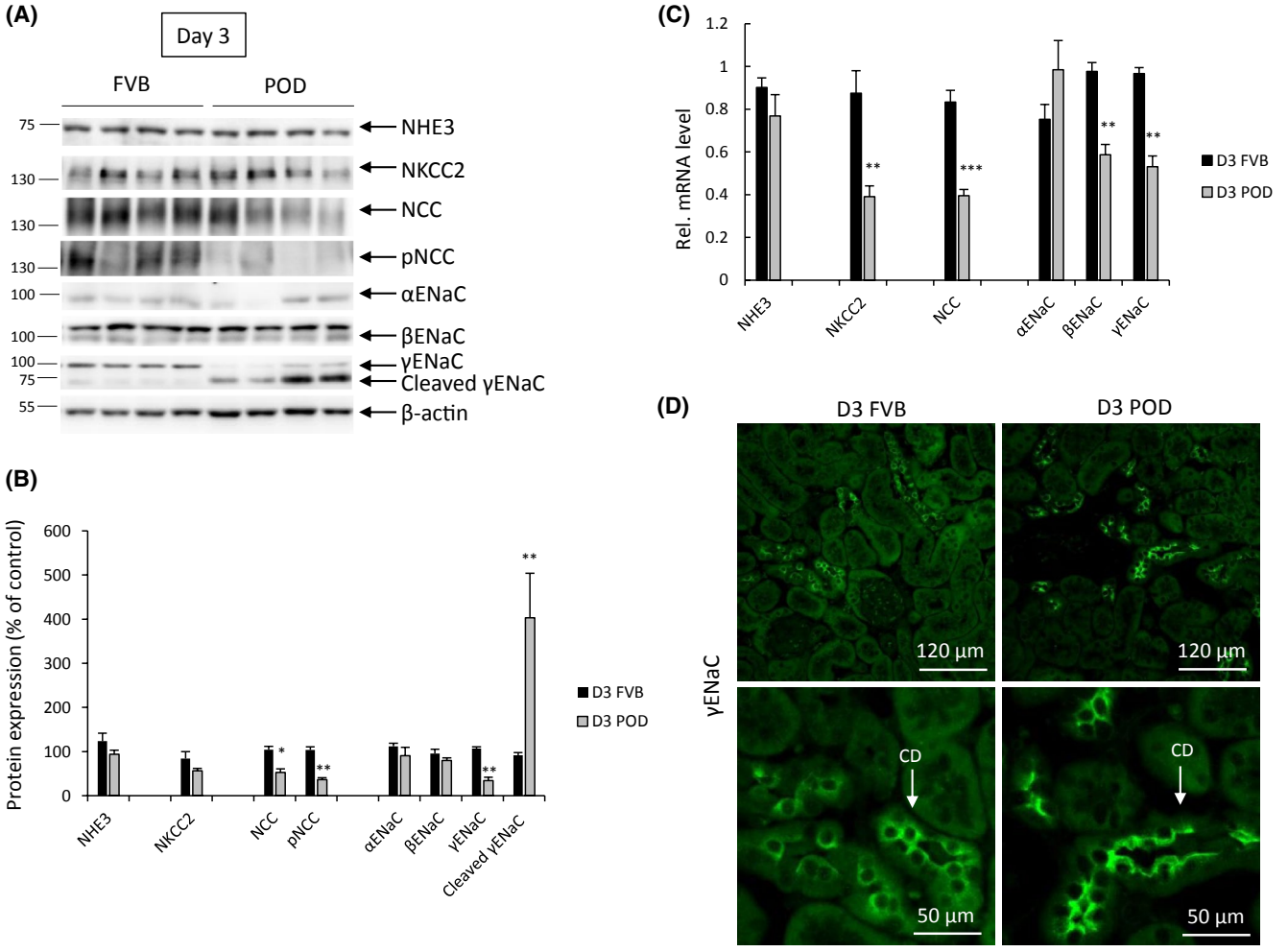

FIGURE 3 Massive cleavage of γ-ENaC during the sodium retention phase in nephrotic syndrome. Three days after intraperitoneal injection of dimerizer, kidneys from nephrotic POD-ATTAC (POD) and control (FVB) mice were harvested. Total proteins and mRNA were extracted from kidney cortices and proteins were separated by SDS-PAGE. Kidneys slices were fixed by immersion and processed for immunohistochemistry. A, Representative Western blot experiment showing the abundance of total and post-translationally modified kidney tubule sodium transporters, namely: NHE3, NKCC2, total and phosphorylated (TP53) NCC, α and β-ENaC, and full-length and cleaved γ-ENaC. β-actin was used as a loading control. B, Bar graph shows the densitometric quantification of Western blots. C, qRT-PCR analysis of variations in the mRNA levels of the main tubular sodium transporters. D, Immunofluorescence imaging of γ-ENaC shows apical localization in principal cells in collecting ducts (CD) of nephrotic POD mice. Values are means ± SEM from 5 mice in each group. POD-ATTAC mice were compared to control mice using a Mann-Whitney test; $*P < .05$, $**P < .01$, $***P < .001$

3.4 | Persisting γ-ENaC cleavage at steady state

Western blot analysis and immunohistochemistry experiments performed at day 5 after dimerizer injection revealed a persistent increase in cleaved γ-ENaC abundance (percentage of controls ± SEM: 214.9 ± 25.1) (Figure 4A,B) associated with increased apical localization in the principal cells of CNT and CD (Figure 4D) in POD-ATTAC mice. This was associated with decreased protein abundance of α-, β-ENaC subunits and full-length γ-ENaC as well as NHE3 and NCC in nephrotic mice (Figure 4A,B). A persistent decrease in NKCC2, NCC, and β- and γ-ENaC mRNA levels was observed (Figure 4C).

3.5 | Increased aquaporin 2 abundance during the early phase of NS

Aquaporin 2 (AQP2) accounts for the rate-limiting step of regulated water reabsorption along the CNT and CD. In POD-ATTAC mice, AQP2 protein levels were increased at days 2 (percentage of controls ± SEM: 168 ± 15) and 3 (percentage of controls ± SEM: 177.3 ± 19.7) and returned to

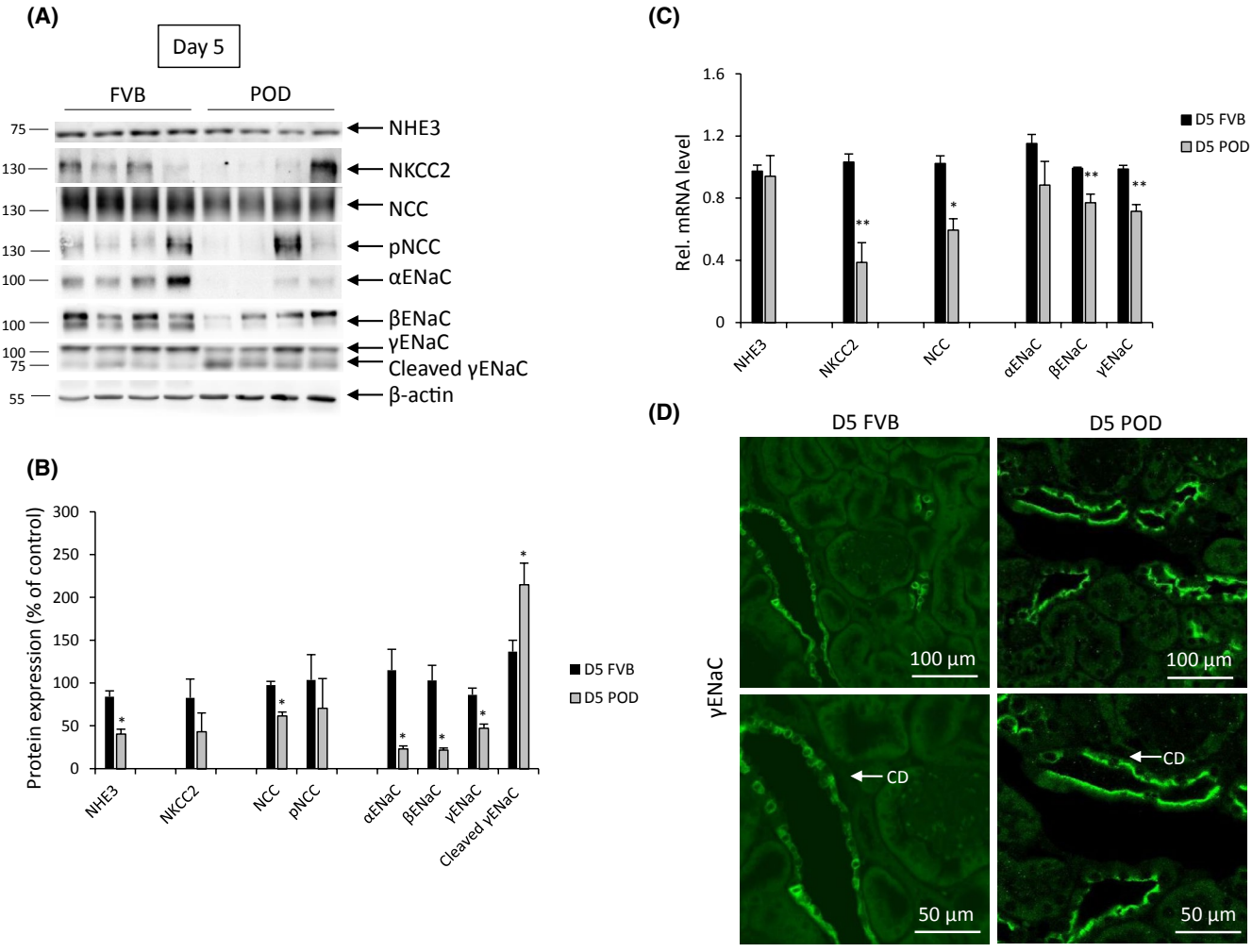

FIGURE 4 Decreased sodium transporters and channels at steady state. Five days after intraperitoneal injection of dimerizer, kidneys from nephrotic POD-ATTAC (POD) and control (FVB) mice were harvested. Total proteins and mRNA were extracted from kidney cortex and proteins were separated by SDS-PAGE. Kidney slices were fixed by immersion and processed for immunohistochemistry. A, Representative Western blot experiment showing the abundance of total and post-translationally modified kidney tubule sodium transporters, namely: NHE3, NKCC2, total and phosphorylated (TP53) NCC, α and β-ENaC, full-length, and cleaved γ-ENaC. β-actin was used as a loading control. B, Bar graph shows the densitometric quantification of Western blots. C, qRT-PCR analysis of variations in the mRNA levels of the main tubular sodium transporters. D, Immunofluorescence imaging of γ-ENaC shows persistent increased apical localization in principal cells in collecting ducts (CD) of nephrotic POD mice. Values are means ± SEM from 5 mice in each group. POD-ATTAC mice were compared to control mice using a Mann-Whitney test; $*P < .05$, $**P < .01$, $***P < .001$

control levels at day 5 after dimerizer injection (Figure 5A,B). Immunofluorescence staining performed at day 3 showed an increased staining and apical localization of AQP2 in the CD (Figure 5D). In addition, after the induction of NS, the mRNA levels of AQP2 were increased at days 2, 3, and 5 whereas hypothalamic vasopressin mRNA levels were unchanged (Figure 5C).

3.6 | Mathematical simulations predict a shift in sodium transport from PCT to ASDN

The observed changes in sodium transporter abundance at each stage and in GFR were incorporated into a mathematical model of transport along the nephron. Sodium transport (Figure 6A) and oxygen consumption (Figure 6B) were predicted to increasingly shift toward the CNT and CCD. The model predicted that sodium transport and oxygen consumption decreased both overall and in the PCT at day 2 in nephrotic compared to control mice, despite the upregulation of sodium transporters. This decrease results from the early impairment of the GFR. The predicted decrease in sodium reabsorption and oxygen consumption in the PCT was further pronounced at days 3 and 5 after induction of NS, whereas sodium transport, oxygen consumption and sodium transport efficiency (Figure 6C) were predicted to increase in both the CNT and CD.

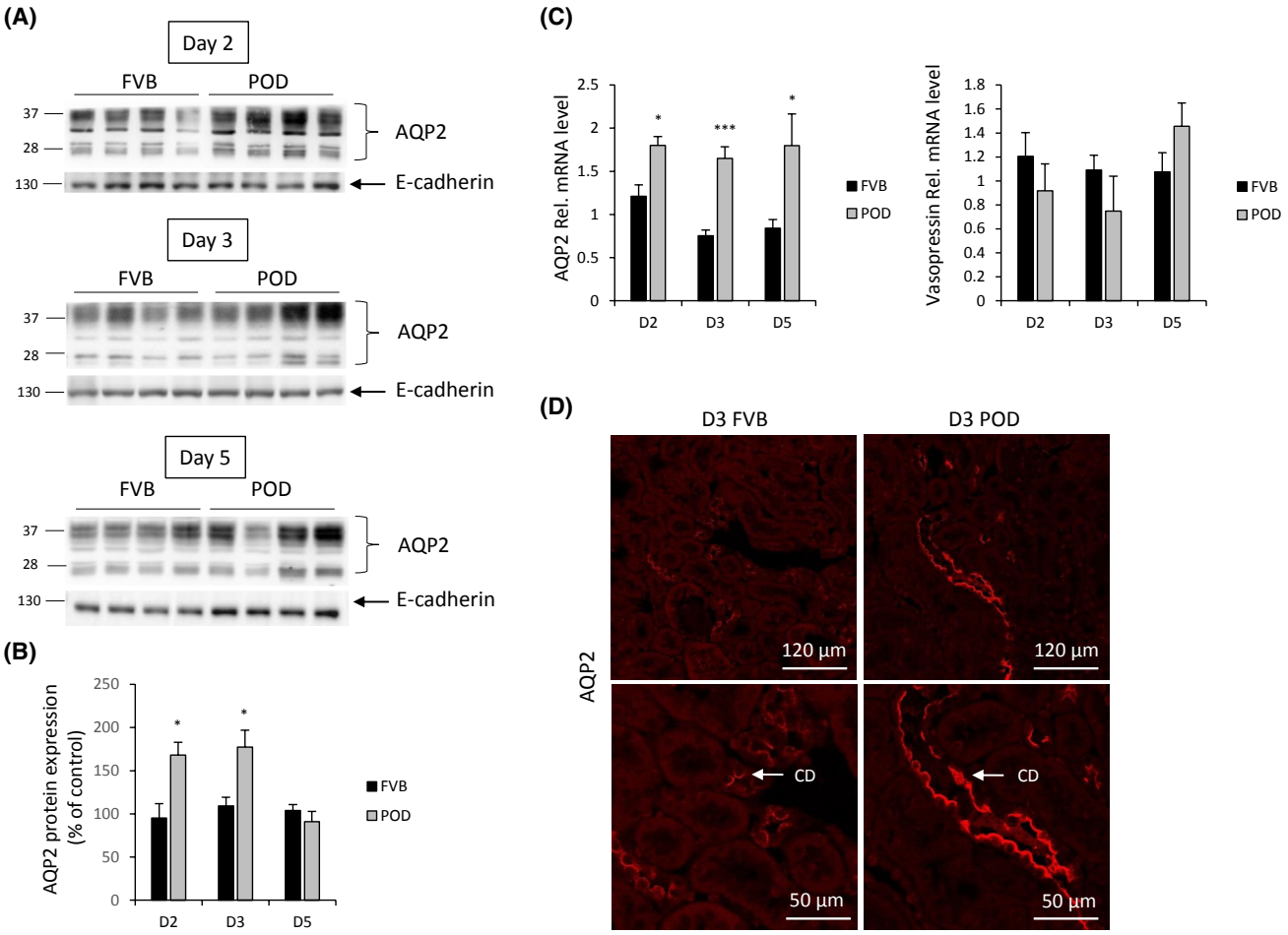

FIGURE 5 Aquaporin protein and mRNA levels increase after the induction of nephrotic syndrome in POD-ATTAC mice. At days 2, 3, and 5 after intraperitoneal injection of dimerizer, kidneys, and hypothalamus from nephrotic POD-ATTAC (POD) and control (FVB) mice were harvested. Total proteins and mRNA from the kidneys and total mRNA from the hypothalamus were extracted and proteins were separated by SDS-PAGE. Kidneys slices were fixed by immersion and processed for immunohistochemistry. A, Representative Western blot experiments showing aquaporin 2 (AQP2) at days 2, 3, and 5. E-cadherin was used as a loading control. B, Bar graph shows the densitometric quantification of Western blots. C, qRT-PCR analysis of variations in the mRNA levels of AQP2 in kidney and hypothalamic preprovasopressin at day 2, 3, and 5. D, Immunofluorescence imaging of AQP2 shows increased staining and apical localization in collecting ducts (CD) of nephrotic POD mice at day 3. Values are means ± SEM from 4 mice in each group. POD-ATTAC mice were compared to control mice using an unpaired Student *t* test; $*P < .05$, $**P < .01$, $***P < .001$

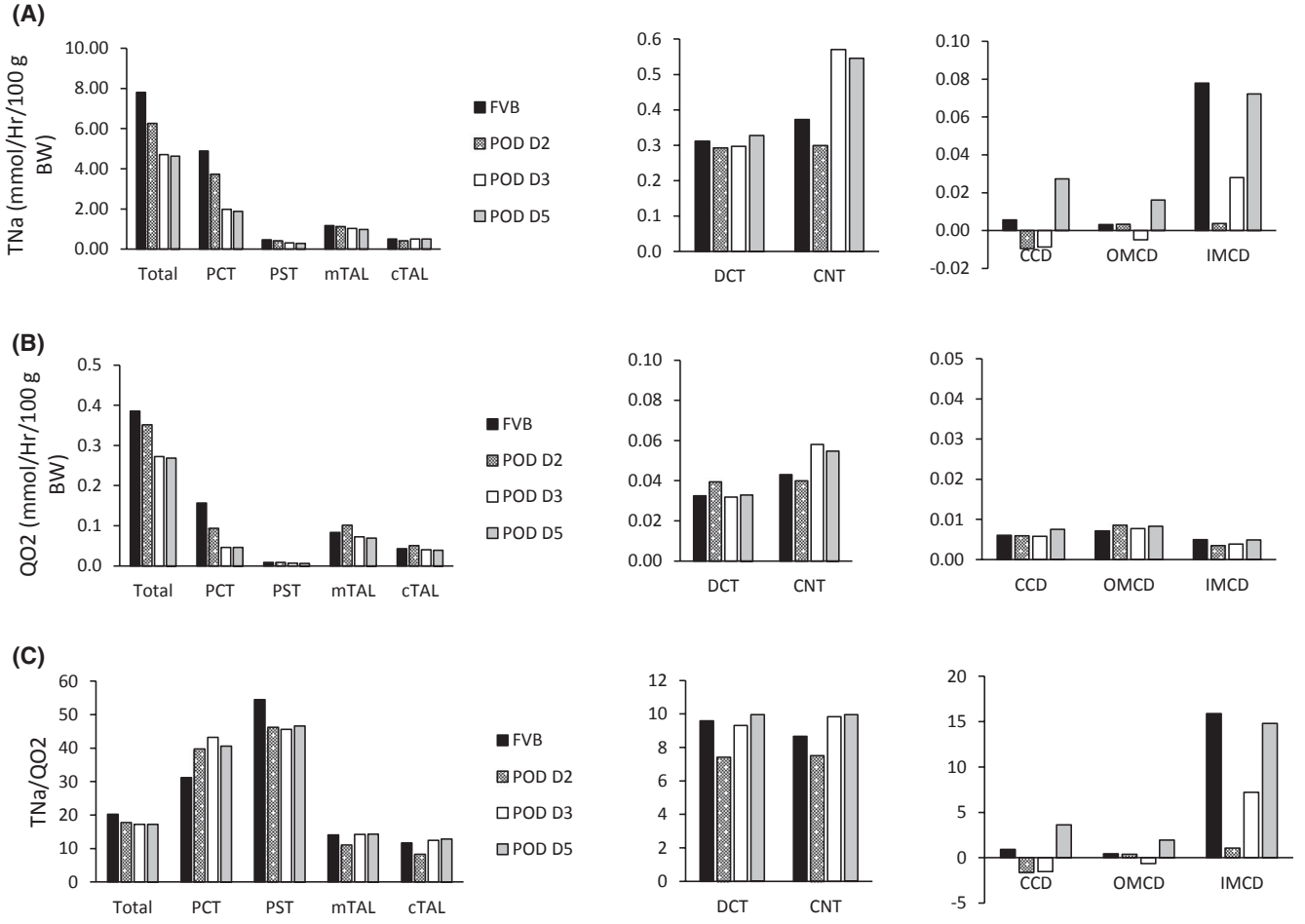

FIGURE 6 Mathematical modeling of sodium transport along the nephron shows the shift in sodium transport from proximal tubules to ASDN. Using an in silico model of sodium transport along the nephron, we computed the rate of sodium transport (TNa; A), the rate of O_2 consumption (QO_2; B) and the efficiency of sodium transport (TNa/QO_2; C) along the nephron of control mice (FVB) and nephrotic POD-ATTAC mice at days 2, (POD D2), 3 (POD D3), and 5 (POD D5) after dimerizer injection. Results account for observed fractional changes in transporter and channel abundance as shown in Figures 2-4. Shown is the predicted TNa (A), QO_2 (B) and TNa/QO_2 (C) for the whole nephron, PCT, PST, cTAL, mTAL, DCT, CNT, CCD, outer medullary (OMCD), and inner medullary (IMCD) collecting duct. Relative to control mice, sodium reabsorption, oxygen consumption, and sodium transport efficiency are predicted to be shifted to the CNT at days 3 and 5 after dimerizer injection in NS mice.

3.7 | Functional diuretic tests confirmed the shift from NCC- to ENaC-dependent sodium retention

We next assessed the function of segment specific sodium transporters by measuring diuretic-induced natriuresis at each day after the induction of glomerular injury. At day 2, the natriuretic response to hydrochlorothiazide, an inhibitor of NCC, and benzamil, an inhibitor of ENaC, were almost equivalent. As expected from Western blotting and immunofluorescence experiments (see Figures 2-4), the efficiency of benzamil compared to that of hydrochlorothiazide was increased at days 3 and 5 (Figure 7A). The ratio of the thiazide-over-benzamil- induced natriuresis (0.8 at day 2, 0.1 at day 3, and 0.3 at day 5) further illustrates this time-dependent shift from NCC- to ENaC-mediated sodium reabsorption in POD-ATTAC mice (Figure 7B).

3.8 | Sodium retention is independent of a rise in plasma aldosterone levels in nephrotic syndrome

Increased plasma aldosterone (mean ± SEM: 1983 ± 333.1 in POD-ATTAC vs 137 ± 33.4 pg/mL in FVB mice, $P = .0009$) and SGK1 mRNA levels (fold controls: 3.2) were increased at day 3 after dimerizer injection (Figure 8A,B) but were similar to control levels at days 2 and 5. This finding suggests that sodium retention observed in POD-ATTAC nephrotic mice at days 2 and 5 was independent of increased plasma aldosterone levels. To further assess the

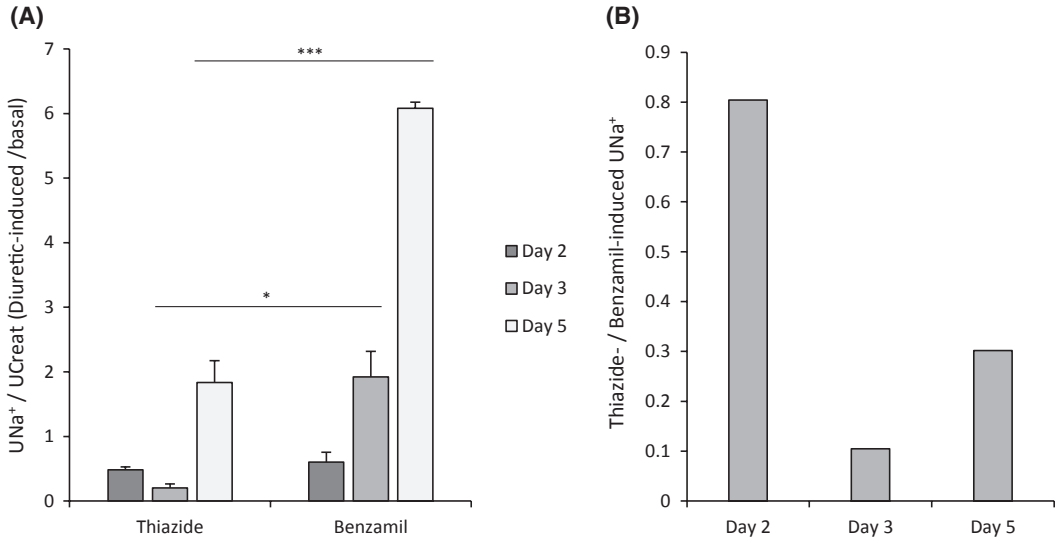

FIGURE 7 Diuretic tests confirm the time-dependent shift from NCC to ENaC activity. Two, three, and five days after intraperitoneal injection of dimerizer, mice were given a single dose of hydrocholorothiazide (Thiazide in the graph) through intraperitoneal injection, which inhibits NCC in the distal convoluted tubule, or benzamil, which inhibits ENaC in the connecting tubule and the collecting duct. Results are expressed as the ratio of diuretic-induced to baseline natriuresis in A and the ratio of hydrochlorothiazide over benzamil-induced natriuresis in B. Values are means ± SEM from 4 mice in each group. Hydrochlorothiazide-induced natriuresis was compared to benzamil-induced natriuresis at each day with an unpaired Student *t* test in A; $*P < .05$, $**P < .01$, $***P < .001$

role of aldosterone in sodium retention in POD-ATTAC mice, control, and nephrotic mice received 50 mg/kg potassium-canrenoate (sc), a competitive antagonist of the MR. Results show that potassium-canrenoate neither prevented ascites (Figure 8C,D) nor reduced the extent of γ-ENaC cleavage in nephrotic POD-ATTAC mice (Figure 8E,F). These findings support the idea that γ-ENaC cleavage and sodium retention are at least partly independent of the transient rise (day 3) in plasma aldosterone levels found in POD-ATTAC mice.

3.9 | Low potassium diet prevented hyperkalemia, NCC dephosphorylation and γ-ENaC cleavage at day 3

POD-ATTAC mice were fed a low potassium diet starting from the day of NS induction to prevent hyperkaliemia. Analyses performed at day 3 showed that low potassium-fed nephrotic mice displayed unchanged plasma potassium levels compared to control FVB mice (Figure 9B). Western blot analysis at day 3 revealed increased NCC protein abundance and phosphorylation levels associated with decreased abundance of cleaved γ-ENaC compared to normal potassium-fed nephrotic mice. As expected, SPAK protein abundance and phosphorylation levels were increased in low potassium fed control FVB mice but were surprisingly decreased in nephrotic mice fed either a low or normal potassium diet (Figure 9B,C). These observations suggest that hyperkaliemia is responsible for the shift from NCC- to ENaC-dependent sodium retention and this occurs independently of SPAK.

4 | DISCUSSION

In this study, we showed that sodium retention occurs in different nephron segments depending on the stage of development of NS, and that potassium intake has an important role in determining the major tubular site of sodium reabsorption in NS.

4.1 | Limitations and advantages of the POD-ATTAC mouse model

We used the POD-ATTAC mouse model[10] to study the early development and time-course of sodium retention along the nephron. With respect to previous mouse models, POD-ATTAC mice do not display the non-specific tubular and/or vascular alterations that can be associated with drug-induced glomerular injuries.[6] These transgenic mice express a FKBP/caspase-8 fusion protein under the control of the podocin promoter.[10] Activation of endogenous caspase-8 by a chemical dimerizer leads to specific and inducible podocyte apoptosis, massive proteinuria, hypoproteinemia, and ascites. The podocyte specific and dose-dependent apoptosis in POD-ATTAC mice closely mimics human glomerular diseases initiated by podocyte injury such as minimal change disease and focal segmental glomerulosclerosis.[10] Unlike the

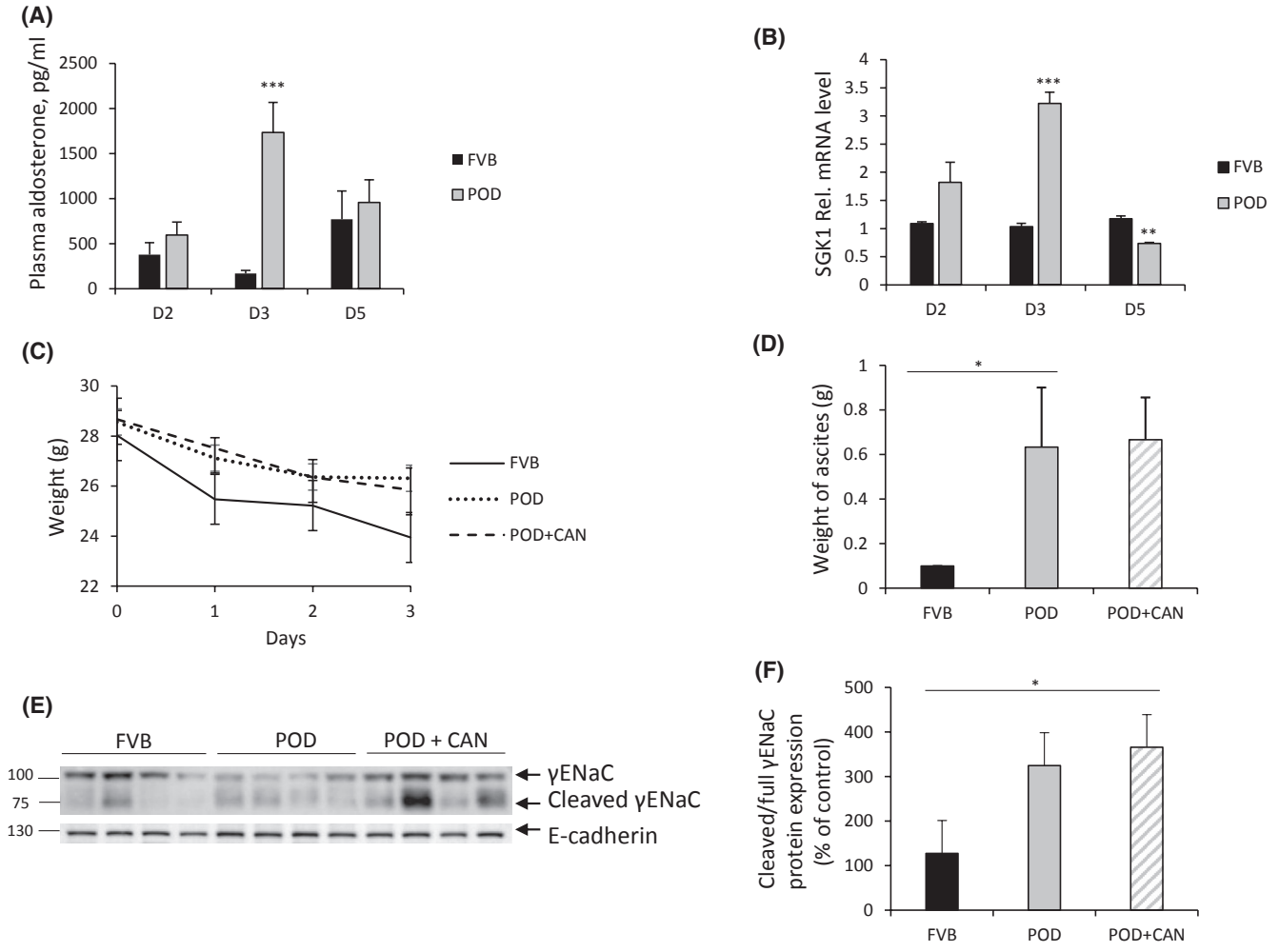

FIGURE 8 Sodium retention is partially independent of aldosterone in nephrotic syndrome. A, Plasma aldosterone levels in controls (FVB) and POD-ATTAC (POD) mice, at days 2, 3, and 5 after dimerizer injection. B, qRT-PCR analysis of variations in the mRNA levels of SGK1 in FVB and POD mice at days 2, 3, and 5 after dimerizer injection. Potassium-canrenoate (CAN) was administered subcutaneously for 5 days starting one day before intraperitoneal injection of the dimerizer. FVB and control POD mice were administered the same volume of 5% glucose subcutaneously. Three days after intraperitoneal injection of the dimerizer, kidneys from control FVB mice and nephrotic POD, treated or untreated with potassium-canrenoate, were harvested. Total proteins were extracted and separated by SDS-PAGE. C, Weight of FVB, POD, and POD+CAN mice. D, Quantification of ascites at day 3 in FVB, POD, and POD+CAN mice. E, Western blotting experiments showing full length and cleaved γ-ENaC of FVB, POD, and POD+CAN mice. E-cadherin was used as a loading control. F, Bar graph shows the densitometric quantification of Western blots. Values are means ± SEM from 4 mice in each group. POD-ATTAC mice were compared to control mice using unpaired Student's *t* test in A and B. POD-ATTAC mice treated with canrenone, without canrenone and control mice were compared using a Kruskal-Wallis test in D and F; $*P < .05$, $**P < .01$, $***P < .001$

constitutive knock-out mice models for podocyte-specific proteins like podocin[9] or nephrin,[8] the POD-ATTAC mice display low early mortality, allowing us to study NS from the onset to the steady-state. Moreover, the nephrotic phenotype of POD-ATTAC mice was reproducible between heterozygotes, whereas the inducible inactivation of podocin in mature kidneys led to phenotypic variability concerning the progression of renal disease.[9] However, the POD-ATTAC mice model possesses several limitations: one of them is the early impairment of renal function after the induction of NS that may partly stem from a prerenal dysfunction due to volume contraction and/or an organic renal dysfunction due to the loss of podocytes. The second limitation is the rapid onset of massive proteinuria within 3 d which is similar to the PAN-induced nephrotic model,[3,4] but more rapid than acquired human diseases.

4.2 | Activation of sodium transporters in PCT and DCT during the early phase of nephrotic syndrome

Based on biological parameters we identified three phases in the development of NS in POD-ATTAC mice: the onset

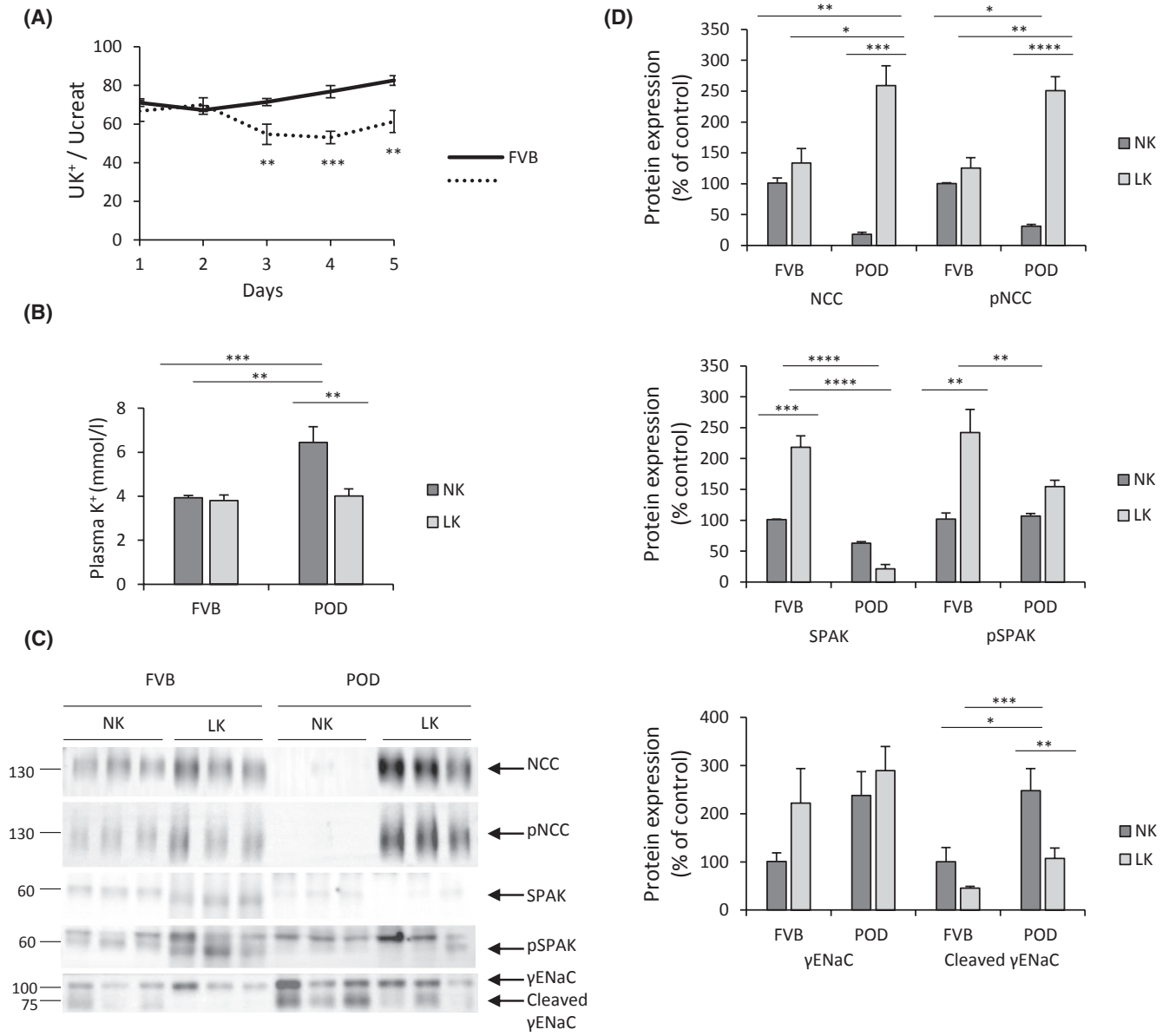

FIGURE 9 Low potassium diet prevented hyperkalemia and the shift in sodium transport from the distal convoluted tubule to the collecting system. A, Urinary potassium excretion. B, Kalemia at day 3 after NS induction in FVB and POD-ATTAC mice fed a normal (NK) or low (LK) potassium diet. C, Representative western blot experiments showing the increased abundance of total and phosphorylated NCC (TP58) and decreased abundance of cleaved γ-ENaC in nephrotic mice fed a LK diet compared to nephrotic mice fed a NK diet. Total and phosphorylated SPAK (pSer373) abundance were increased in FVB mice fed with LK but not in nephrotic mice fed with either NK or LK. D, Bar graph shows densitometric quantification of Western blots, normalized with Coomassie staining. Values are means ± SEM from 3-8 mice in each group. The four groups: FVB NK, FVB LK, POD-ATTAC NK, and POD-ATTAC LK were compared with one-way ANOVA. *$P < .05$, **$P < .01$, ***$P < .001$

of proteinuria occurring at day 2, massive proteinuria and sodium retention occurring at day 3, and the initiation of a steady-state at day 5. At day 2, when nephrotic POD-ATTAC mice displayed hypovolemia associated with proteinuria, we found increased NHE3 protein levels and phosphorylated NCC. These sodium transporters are regulated by the SRAA, which is activated under hypovolemia. NHE3 is up-regulated by the physiological concentration of angiotensin II.[15] A recent work showed that filtered angiotensinogen is reabsorbed by megalin in the PCT in another model of podocyte injury and non-selective proteinuria.[16,17] Angiotensinogen is then converted into angiotensin II and locally increases NHE3 protein abundance, enhancing sodium reabsorption in the PCT.[16] NCC is also regulated by angiotensin II and aldosterone.[18] In our study, plasma aldosterone abundance were unchanged at day 2 but may exert permissive effects. Moreover, angiotensin II was shown to activate NCC in a WNK (with-no-lysine kinases) 4-dependent manner.[19] The mRNA levels of sodium channels and transporters were unchanged at day 2. This

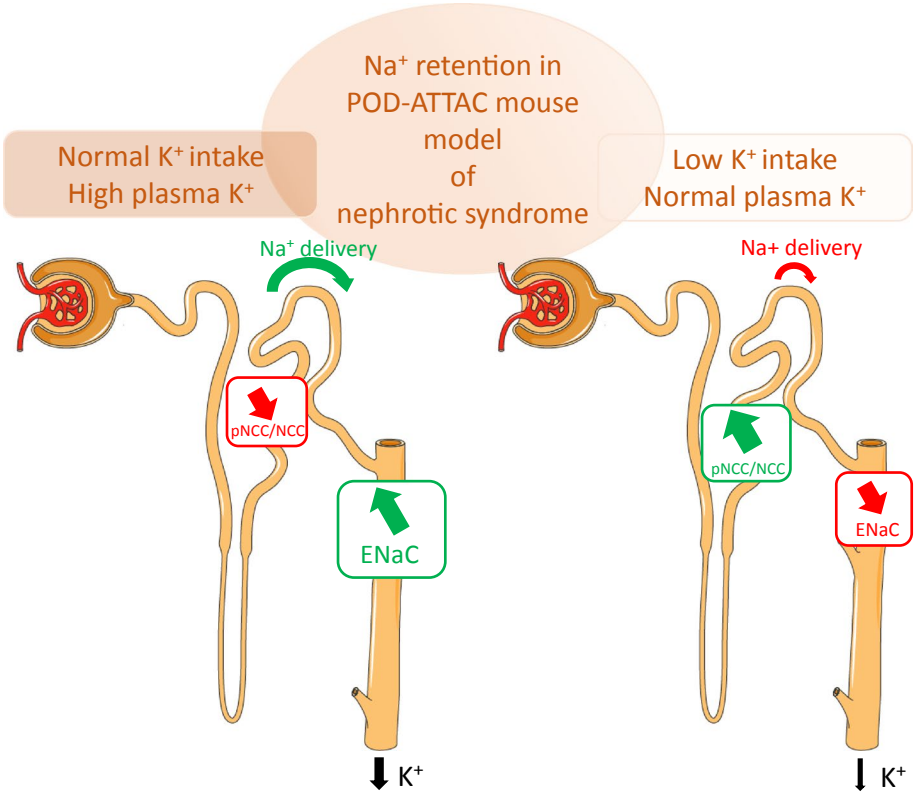

FIGURE 10 Illustrative summary. Images are from Servier Smart Medical Art.

uncoupling between mRNA and protein levels may indicate that observed increases in NHE3 and NKCC2 (although non-significant) protein abundance may rely on increased mRNA translation or decreased protein degradation. The latter is more likely since regulation of protein abundance via modulation of protein degradation rate has been demonstrated for several sodium transporters such as the sodium/phosphate cotransporter NaPi-2[20] and the Na,K-ATPase.[21]

4.3 | Hyperkalemia induces the shift from upstream segments to the ASDN

Three days after the induction of podocyte loss, GFR decreased by 50% and hyperkalemia associated with low kaliuresis, indicating a renal origin, was observed. Results suggest a shift in sodium retention from the PCT and DCT at day 2 to the CNT and CD at day 3, as indicated by the normalized abundance of NHE3, decreased abundance of NCC and phosphorylated NCC, and increased abundance of cleaved γ-ENaC. This shift was prevented by a low potassium diet supporting the hypothesis that potassium homeostasis is a major determinant of the tubular site of sodium reabsorption in NS.

Hyperkalemia may promote the decrease in phosphorylated NCC at day 3 in order to increase sodium and fluid delivery to the potassium-secreting segment of the kidney tubule, ie, the DCT2, CNT, and CD. The increased sodium concentration in the fluid delivered to the distal nephron stimulates the entry of sodium through ENaC, thereby augmenting the lumen-negative transepithelial potential that drives the secretion of potassium through ROMK/BK channels. The aldosterone paradox states that the regulation of renal handling of potassium prevails over that of sodium along the kidney tubule. Thus, NCC is inhibited under a large potassium load even when associated with sodium depletion, in order to increase potassium secretion by the distal parts of the nephron. This mechanism is directly mediated by local WNK activity, resulting in the decoupling of NCC and ENaC in ASDN as a first defense against potassium variations.[22] WNK 1, 3, and 4 are expressed in the kidney and are inhibited by high intracellular chloride resulting from high extracellular potassium. The binding of chloride prevents the activation of WNK by autophosphorylation, leading to a SPAK-dependent inhibition of NCC.[23] In FVB control mice fed a low potassium diet, we observed the expected activation of SPAK and NCC. Since plasma potassium did not detectably decrease and underwent little variation, this SPAK activation is likely due to "feed-forward" control of potassium homeostasis (Figure 10). Indeed, "feed-forward" system aims to prevent rises of potassium levels after an oral load, independently of plasma potassium and aldosterone,[24] as opposed to the "feedback" control. Nephrotic POD-ATTAC mice fed a normal potassium diet showed high plasma potassium levels

and decreased NCC/SPAK abundance and phosphorylation, as expected. In this case, the "feedback" control of potassium homeostasis may have prevailed since potassium intake was normal (Figure 10).[24] Surprisingly, despite increased protein levels of NCC and phosphorylated NCC, SPAK, and phosphorylated SPAK levels were decreased in nephrotic POD-ATTAC mice fed a low potassium diet. Since urinary potassium excretion was decreased in these mice, plasma potassium did not change compared with control FVB mice. Since extracellular potassium does not change, one can speculate that intracellular chloride and WNK/SPAK activities did not change as well. These results raise the hypothesis of a SPAK-independent activation of NCC.

4.4 | γ-ENaC cleavage correlates with massive sodium retention in NS

According to literature, ENaC plays a key role in sodium retention in NS. Our results show that α- and β-subunits were either unchanged or decreased in POD-ATTAC mice, but that cleaved γ-subunit abundance was increased when sodium retention was massive. We have shown previously that overexpressing γ-ENaC in cultured CD principal cells increased ENaC apical expression and activity.[21,25] We confirmed the importance of the γ-subunit in ENaC activity in our model with diuretic tests that showed the increase in benzamil-induced compared to hydrochlorothiazide-induced natriuresis accompanying the increase in cleaved γ-ENaC. Regulation of γ-ENaC involves its cleavage by proteases in order to increase its open probability and its cell surface expression.[26] Increased cleavage of ENaC subunits associated with decreased mRNA and uncleaved protein levels in POD-ATTAC mice at days 3 and 5 after induction of NS implies a stimulation of the proteolytic maturation of pre-existing ENaC subunits. γ-ENaC may be cleaved by intracellular furin, extracellular membrane-bound proteases like CAP1/prostasin, and soluble proteases. We detected a 75 kDa fragment possibly accompanied by a 70 kDa fragment of γ-ENaC with an antibody reacting with the C-terminal part, which is compatible with furin[27] and CAP1/prostasin[28] cleavage. It has been shown that soluble extracellular proteases present in nephrotic urine may also cleave γ-ENaC in mice and humans.[3] At day 3, nephrotic mice still displayed biological parameters indicative of relative hypovolemia such as increased hematocrit and hemoglobin. Sodium restriction is a strong activator of γ-ENaC cleavage in rats.[29] This process is dependent on aldosterone as evinced by the finding that rats subjected to aldosterone infusion displayed increased cleaved γ-ENaC within 3 hours after the beginning of infusion. The results suggest that aldosterone induces the rapid cleavage and apical addressing of ENaC.[30] Moreover, the cleaved γ-subunit is absent in kidney tubule-specific MR knockout mice.[31] However, the mechanism of γ-ENaC cleavage in NS is still debated.

4.5 | Aldosterone-independent regulation of sodium retention

According to the underfilling theory, aldosterone plays a central role in sodium retention because relative hypovolemia is frequently associated with NS, stimulating RAAS and thus aldosterone secretion. However, sodium retention persisted in aldosterone-clamped PAN rats,[5] and sodium retention took place only in the nephrotic kidney in the case of unilateral PAN injection.[32] Furthermore, nephrotic mice displayed high plasma aldosterone and increased mRNA levels of the aldosterone target gene SGK1 at day 3 but normal levels of both were observed when urinary sodium was reduced at day 2. We have also shown that canrenone administration to nephrotic mice did not prevent ascites, weight gain, nor γ-ENaC cleavage at day 3, as previously shown in mice subjected to doxorubicin-induced NS.[33] Those results suggest at least a partial independence of sodium retention from increased plasma aldosterone levels and mineralocorticoid receptor activation. However, aldosterone may participate in the decoupling of NCC and ENaC at day 3 via SGK1, which phosphorylates WNK4 in the DCT thus preventing WNK4-dependent ENaC endocytosis.[34] These results reveal a complex local regulation and interplay between transporters and channels in NS where aldosterone may exert a permissive effect.

4.6 | Mechanism of water retention

Apical cell surface expression of AQP2 is rate-limiting for water permeability of the CD.[35] At days 2 and 3, increased AQP-2 mRNA and protein levels together with hyponatremia indicate water retention accompanying sodium retention during the hypovolemic period of NS. Vasopressin is the major controller of AQP2 expression and apical targeting.[36] Surprisingly, at any stage of NS, hypothalamic vasopressin mRNA levels were not increased in nephrotic mice compared to control mice in our study. On one hand, we cannot exclude an early and transient increase in vasopressin mRNA levels. However, vasopressin has a short half-life that makes long lasting effects unlikely. On the other hand, AQP2 protein expression is regulated by other factors which are relevant in our study, such as aldosterone,[37] and interstitial tonicity[38] generated by avid sodium chloride reabsorption. Therefore, the observed increase in AQP2 expression is likely independent of increased vasopressin secretion.

Normalization of plasma sodium concentration and AQP2 protein levels at day 5 contrasted with the persisting increase of AQP2 mRNA levels. Uncoupling between AQP2 protein and mRNA levels in the cortex has been described in certain conditions in rats for instance such as fasting.[39] Nephrotic and control mice displayed similar amounts of water and food intake compared to FVB mice (Supplementary Figure 1), suggesting that another mechanism of uncoupling is at work. Moreover, this observation indicates that the central control of thirst or sodium appetite[40] of hypovolemic nephrotic mice was not a major contributor in the altered sodium and water balance in our study. Our results rather suggest that intrarenal mechanisms are at work to drive massive sodium and water retention.

5 | CONCLUSIONS

The POD-ATTAC mouse model, despite its limitations, reveals that sodium retention in NS is a continuous process and can occur in different segments of the nephron, depending on hemodynamics, GFR, and plasma potassium. In this model, the underfilling mechanism dominates and potassium balance requirements determine the site of sodium reabsorption in NS. Aldosterone may play a permissive role in the shift from the DCT to ASDN and in the activation of ENaC under conditions of hyperkalemia.

ACKNOWLEDGMENTS

This work was supported by the National Center of Competence in Research Kidney control of homeostasis and a Swiss National Science Foundation grant 31003A_156736/1 and 31003A_175471/1 to EF and 310030_143929/1 to JL. KU received funding within the frame of IKPP2 from the European Union's Seventh Framework Program for research, technological development and demonstration under grant agreement no 608847.

CONFLICT OF INTEREST

The authors declare no conflicts of interest.

AUTHOR CONTRIBUTIONS

E. Feraille, E. Dizin, and S. de Seigneux. designed the study, E. Dizin, V. Olivier, C. Maire, O. Komarynets, A. Sassi, J. Loffing, J. M. Rutkowski, M. Maillard, I. Roth, and A. Edwards carried out experiments, E. Dizin, V. Olivier analyzed the data, C. Maire, V. Olivier, and A. Edwards made the figures, E. Feraille, V. Olivier, J.M. Rutkowski, A. Sassi, and A. Edwards drafted and revised the paper, all authors approved the final version of the manuscript.

REFERENCES

1. Siddall EC, Radhakrishnan J. The pathophysiology of edema formation in the nephrotic syndrome. *Kidney Int*. 2012;82:635-642.
2. Humphreys MH. Mechanisms and management of nephrotic edema. *Kidney Int*. 1994;45:266-281.
3. Svenningsen P, Bistrup C, Friis UG, et al. Plasmin in nephrotic urine activates the epithelial sodium channel. *J Am Soc Nephrol JASN*. 2009;20:299-310.
4. Deschênes G, Doucet A. Collecting duct (Na+/K+)-ATPase activity is correlated with urinary sodium excretion in rat nephrotic syndromes. *J Am Soc Nephrol JASN*. 2000;11:604-615.
5. Lourdel S, Loffing J, Favre G, et al. Hyperaldosteronemia and activation of the epithelial sodium channel are not required for sodium retention in puromycin-induced nephrosis. *J Am Soc Nephrol JASN*. 2005;16:3642-3650.
6. Kim SW, Wang W, Nielsen J, et al. Increased expression and apical targeting of renal ENaC subunits in puromycin aminonucleoside-induced nephrotic syndrome in rats. *Am J Physiol Renal Physiol*. 2004;286:F922-F935.
7. de Seigneux S, Kim SW, Hemmingsen SC, Frøkiaer J, Nielsen S. Increased expression but not targeting of ENaC in adrenalectomized rats with PAN-induced nephrotic syndrome. *Am J Physiol Renal Physiol*. 2006;291:F208-F217.
8. Putaala H, Soininen R, Kilpeläinen P, Wartiovaara J, Tryggvason K. The murine nephrin gene is specifically expressed in kidney, brain and pancreas: inactivation of the gene leads to massive proteinuria and neonatal death. *Hum Mol Genet*. 2001;10:1-8.
9. Mollet G, Ratelade J, Boyer O, et al. Podocin inactivation in mature kidneys causes focal segmental glomerulosclerosis and nephrotic syndrome. *J Am Soc Nephrol JASN*. 2009;20:2181-2189.
10. Rutkowski JM, Wang ZV, Park ASD, et al. Adiponectin promotes functional recovery after podocyte ablation. *J Am Soc Nephrol JASN*. 2013;24:268-282.
11. Schreiber A, Shulhevich Y, Geraci S, et al. Transcutaneous measurement of renal function in conscious mice. *Am J Physiol Renal Physiol*. 2012;303:F783-F788.
12. Udwan K, Abed A, Roth I, et al. Dietary sodium induces a redistribution of the tubular metabolic workload. *J Physiol*. 2017;595(22):6905-6922.
13. Nlandu Khodo S, Dizin E, Sossauer G, et al. NADPH-oxidase 4 protects against kidney fibrosis during chronic renal injury. *J Am Soc Nephrol JASN*. 2012;23:1967-1976.
14. Layton AT, Vallon V, Edwards A. Predicted consequences of diabetes and SGLT inhibition on transport and oxygen consumption along a rat nephron. *Am J Physiol Renal Physiol*. 2016;310:F1269-F1283.
15. Houillier P, Chambrey R, Achard JM, Froissart M, Poggioli J, Paillard M. Signaling pathways in the biphasic effect of angiotensin II on apical Na/H antiport activity in proximal tubule. *Kidney Int*. 1996;50:1496-1505.
16. Koizumi M, Ueda K, Niimura F, et al. (2019) Podocyte injury augments intrarenal angiotensin II generation and sodium retention in a megalin-dependent manner. *Hypertens Dallas Tex*. 1979;74:509-517.
17. Motoyoshi Y, Matsusaka T, Saito A, et al. Megalin contributes to the early injury of proximal tubule cells during nonselective proteinuria. *Kidney Int*. 2008;74:1262-1269.
18. Kim GH, Masilamani S, Turner R, Mitchell C, Wade JB, Knepper MA. The thiazide-sensitive Na-Cl cotransporter is an aldosterone-induced protein. *Proc Natl Acad Sci USA*. 1998;95:14552-14557.
19. Castañeda-Bueno M, Cervantes-Pérez LG, Vázquez N, et al. Activation of the renal $Na^+:Cl^-$ cotransporter by

angiotensin II is a WNK4-dependent process. *Proc Natl Acad Sci USA*. 2012;109:7929-7934.
20. Pfister MF, Lederer E, Forgo J, et al. Parathyroid hormone-dependent degradation of type II Na+/Pi cotransporters. *J Biol Chem*. 1997;272:20125-20130.
21. Wang Y-B, Leroy V, Maunsbach AB, et al. Sodium transport is modulated by p38 kinase-dependent cross-talk between ENaC and Na, K-ATPase in collecting duct principal cells. *J Am Soc Nephrol JASN*. 2014;25:250-259.
22. Arroyo JP, Ronzaud C, Lagnaz D, Staub O, Gamba G. Aldosterone paradox: differential regulation of ion transport in distal nephron. *Physiol Bethesda Md*. 2011;26:115-123.
23. Terker AS, Zhang C, Erspamer KJ, Gamba G, Yang C-L, Ellison DH. Unique chloride-sensing properties of WNK4 permit the distal nephron to modulate potassium homeostasis. *Kidney Int*. 2016;89:127-134.
24. Youn JH. Gut sensing of potassium intake and its role in potassium homeostasis. *Semin Nephrol*. 2013;33:248-256.
25. Volk KA, Husted RF, Sigmund RD, Stokes JB. Overexpression of the epithelial Na+ channel gamma subunit in collecting duct cells: interactions of Liddle's mutations and steroids on expression and function. *J Biol Chem*. 2005;280:18348-18354.
26. Frindt G, Ergonul Z, Palmer LG. Surface expression of epithelial Na channel protein in rat kidney. *J Gen Physiol*. 2008;131:617-627.
27. Hughey RP, Mueller GM, Bruns JB, et al. Maturation of the epithelial Na+ channel involves proteolytic processing of the alpha- and gamma-subunits. *J Biol Chem*. 2003;278:37073-37082.
28. Bruns JB, Carattino MD, Sheng S, et al. Epithelial Na+ channels are fully activated by furin- and prostasin-dependent release of an inhibitory peptide from the gamma-subunit. *J Biol Chem*. 2007;282:6153-6160.
29. Frindt G, Palmer LG. Surface expression of sodium channels and transporters in rat kidney: effects of dietary sodium. *Am J Physiol Renal Physiol*. 2009;297:F1249-F1255.
30. Frindt G, Palmer LG. Acute effects of aldosterone on the epithelial Na channel in rat kidney. *Am J Physiol Renal Physiol*. 2015;308:F572-F578.
31. Terker AS, Yarbrough B, Ferdaus MZ, et al. Direct and indirect mineralocorticoid effects determine distal salt transport. *J Am Soc Nephrol JASN*. 2016;27:2436-2445.
32. Ichikawa I, Rennke HG, Hoyer JR, et al. Role for intrarenal mechanisms in the impaired salt excretion of experimental nephrotic syndrome. *J Clin Invest*. 1983;71:91-103.
33. Bohnert BN, Menacher M, Janessa A, et al. Aprotinin prevents proteolytic epithelial sodium channel (ENaC) activation and volume retention in nephrotic syndrome. *Kidney Int*. 2018;93:159-172.
34. Ring AM, Leng Q, Rinehart J, et al. An SGK1 site in WNK4 regulates Na+ channel and K+ channel activity and has implications for aldosterone signaling and K+ homeostasis. *Proc Natl Acad Sci USA*. 2007;104:4025-4029.
35. Nielsen S, Frøkiaer J, Marples D, Kwon T-H, Agre P, Knepper MA. Aquaporins in the kidney: from molecules to medicine. *Physiol Rev*. 2002;82:205-244.
36. Kim JK, Michel JB, Soubrier F, Durr J, Corvol P, Schrier RW. Arginine vasopressin gene expression in chronic cardiac failure in rats. *Kidney Int*. 1990;38:818-822.
37. Hasler U, Mordasini D, Bianchi M, Vandewalle A, Féraille E, Martin P-Y. Dual influence of aldosterone on AQP2 expression in cultured renal collecting duct principal cells. *J Biol Chem*. 2003;278:21639-21648.
38. Hasler U, Leroy V, Jeon US, et al. NF-kappaB modulates aquaporin-2 transcription in renal collecting duct principal cells. *J Biol Chem*. 2008;283:28095-28105.
39. Amlal H, Chen Q, Habo K, Wang Z, Soleimani M. Fasting downregulates renal water channel AQP2 and causes polyuria. *Am J Physiol Renal Physiol*. 2001;280:F513-F523.
40. Jarvie BC, Palmiter RD. HSD2 neurons in the hindbrain drive sodium appetite. *Nat Neurosci*. 2017;20:167-169.
41. Biemesderfer D, Rutherford PA, Nagy T, Pizzonia JH, Abu-Alfa AK, Aronson PS. Monoclonal antibodies for high-resolution localization of NHE3 in adult and neonatal rat kidney. *Am J Physiol*. 1997;273:F289-F299.
42. Wagner CA, Loffing-Cueni D, Yan Q, et al. Mouse model of type II Bartter's syndrome. II. Altered expression of renal sodium- and water-transporting proteins. *Am J Physiol Renal Physiol*. 2008;294:F1373-F1380.
43. Sorensen MV, Grossmann S, Roesinger M, et al. Rapid dephosphorylation of the renal sodium chloride cotransporter in response to oral potassium intake in mice. *Kidney Int*. 2013;83:811-824.

SUPPORTING INFORMATION

Additional supporting information may be found online in the Supporting Information section.

How to cite this article: Dizin E, Olivier V, Maire C, et al. Time-course of sodium transport along the nephron in nephrotic syndrome: The role of potassium. *The FASEB Journal*. 2019;00:1–17. https://doi.org/10.1096/fj.201901345R